doi:10.1038/nature11096

The suppression of star formation by powerful active galactic nuclei

M. J. Page[1], M. Symeonidis[1], J. D. Vieira[2], B. Altieri[3], A. Amblard[4], V. Arumugam[5], H. Aussel[6], T. Babbedge[7], A. Blain[8], J. Bock[2,9], A. Boselli[10], V. Buat[10], N. Castro-Rodríguez[11,12], A. Cava[13], P. Chanial[6], D. L. Clements[7], A. Conley[14], L. Conversi[3], A. Cooray[2,15], C. D. Dowell[2,9], E. N. Dubois[16], J. S. Dunlop[5], E. Dwek[17], S. Dye[18], S. Eales[19], D. Elbaz[6], D. Farrah[16], M. Fox[7], A. Franceschini[20], W. Gear[19], J. Glenn[14,21], M. Griffin[19], M. Halpern[22], E. Hatziminaoglou[23], E. Ibar[24], K. Isaak[25], R. J. Ivison[5,24], G. Lagache[26], L. Levenson[2,9], N. Lu[2,27], S. Madden[6], B. Maffei[28], G. Mainetti[20], L. Marchetti[20], H. T. Nguyen[2,9], B. O'Halloran[7], S. J. Oliver[16], A. Omont[29], P. Panuzzo[6], A. Papageorgiou[19], C. P. Pearson[30,31], I. Pérez-Fournon[11,12], M. Pohlen[19], J. I. Rawlings[1], D. Rigopoulou[30,32], L. Riguccini[6], D. Rizzo[7], G. Rodighiero[20], I. G. Roseboom[5,16], M. Rowan-Robinson[7], M. Sánchez Portal[3], B. Schulz[2,27], D. Scott[22], N. Seymour[1,33], D. L. Shupe[2,27], A. J. Smith[16], J. A. Stevens[34], M. Trichas[35], K. E. Tugwell[1], M. Vaccari[20], I. Valtchanov[3], M. Viero[2], L. Vigroux[29], L. Wang[16], R. Ward[16], G. Wright[24], C. K. Xu[2,27] & M. Zemcov[2,9]

The old, red stars that constitute the bulges of galaxies, and the massive black holes at their centres, are the relics of a period in cosmic history when galaxies formed stars at remarkable rates and active galactic nuclei (AGN) shone brightly as a result of accretion onto black holes. It is widely suspected, but unproved, that the tight correlation between the mass of the black hole and the mass of the stellar bulge[1] results from the AGN quenching the surrounding star formation as it approaches its peak luminosity[2–4]. X-rays trace emission from AGN unambiguously[5], whereas powerful star-forming galaxies are usually dust-obscured and are brightest at infrared and submillimetre wavelengths[6]. Here we report submillimetre and X-ray observations that show that rapid star formation was common in the host galaxies of AGN when the Universe was 2–6 billion years old, but that the most vigorous star formation is not observed around black holes above an X-ray luminosity of 10^{44} ergs per second. This suppression of star formation in the host galaxy of a powerful AGN is a key prediction of models in which the AGN drives an outflow[7–9], expelling the interstellar medium of its host and transforming the galaxy's properties in a brief period of cosmic time.

Measuring star formation in galaxies containing powerful AGN has long been a problem, because the radiation from the AGN outshines that from star formation in almost all wavebands. Of all parts of the electromagnetic spectrum, the far-infrared to millimetre waveband offers the best opportunity to measure star formation in galaxies hosting AGN because, in contrast to strongly star-forming galaxies, AGN emit comparatively little radiation at these wavelengths[10]. The combination of deep X-ray and submillimetre observations therefore offers the best prospects for studying the association of star formation and accretion during the $1 < z < 3$ epoch (2–6 billion years after the Big Bang) when star formation and black hole growth in massive galaxies were at their most vigorous (z is redshift).

The X-ray catalogue of the Chandra Deep Field North (hereafter CDF-N) derives from a series of observations made with the Chandra X-ray observatory with a total of 2×10^6 s exposure time[11]. We restrict the sample to those sources detected in the most penetrating (2–8 keV) band to minimize the influence of obscuration on our results, and we further limit the sample to those sources (64%) for which spectroscopic redshifts are available in the literature[12,13]. Luminosities in the 2–8 keV band were calculated assuming that AGN X-ray spectra are power laws of the form[14] $S_\nu \propto \nu^{-0.9}$ where ν is frequency and S_ν is flux density; the luminosities are not corrected for absorption intrinsic to the AGN or their host galaxies. In order to restrict the X-ray sample to AGN, we have discarded any sources with 2–8 keV luminosity $L_X < 10^{42}$ erg s^{-1}. Submillimetre observations (by the SPIRE[15] instrument on the Herschel Space Observatory) of the CDF-N were carried out in October 2009 as part of the HerMES programme[16]. Maps and source catalogues at wavelengths of 250, 350 and 500 μm were constructed[17]. At the depth of the SPIRE maps, the dominant source of uncertainty in the maps is confusion noise due to the high sky density of sources. For cross-matching with the Chandra source catalogue[11] we chose the 250 μm catalogue, which has the most precise positions, and we used only sources with 250 μm flux densities greater than 18 mJy, which corresponds to a signal-to-noise ratio greater than 3 when the effects of confusion are included[17]. X-ray sources were matched to 250 μm sources within 6 arcsec, corresponding to approximately 95% confidence in the 250 μm positions. The detection statistics are given in Table 1. The expected level of spurious associations between X-ray and 250 μm sources was calculated from the sky density of

[1]Mullard Space Science Laboratory, University College London, Holmbury St Mary, Dorking, Surrey RH5 6NT, UK. [2]California Institute of Technology, 1200 East California Boulevard, Pasadena, California 91125, USA. [3]Herschel Science Centre, European Space Astronomy Centre, Villanueva de la Cañada, 28691 Madrid, Spain. [4]NASA, Ames Research Center, Moffett Field, California 94035, USA. [5]Institute for Astronomy, University of Edinburgh, Royal Observatory, Blackford Hill, Edinburgh EH9 3HJ, UK. [6]Laboratoire AIM-Paris-Saclay, CEA/DSM/Irfu – CNRS – Université Paris Diderot, CE-Saclay, pt courrier 131, F-91191 Gif-sur-Yvette, France. [7]Astrophysics Group, Imperial College London, Blackett Laboratory, Prince Consort Road, London SW7 2AZ, UK. [8]Department of Physics and Astronomy, University of Leicester, University Road, Leicester LE1 7RH, UK. [9]Jet Propulsion Laboratory, 4800 Oak Grove Drive, Pasadena, California 91109, USA. [10]Laboratoire d'Astrophysique de Marseille, OAMP, Université Aix-Marseille, CNRS, 38 rue Frédéric Joliot-Curie, 13388 Marseille cedex 13, France. [11]Instituto de Astrofísica de Canarias (IAC), E-38200 La Laguna, Tenerife, Spain. [12]Departamento de Astrofísica, Universidad de La Laguna (ULL), E-38205 La Laguna, Tenerife, Spain. [13]Departamento de Astrofísica, Facultad de CC Físicas, Universidad Complutense de Madrid, E-28040 Madrid, Spain. [14]Center for Astrophysics and Space Astronomy 389-UCB, University of Colorado, Boulder, Colorado 80309, USA. [15]Department of Physics and Astronomy, University of California, Irvine, California 92697, USA. [16]Astronomy Centre, Department of Physics and Astronomy, University of Sussex, Brighton BN1 9QH, UK. [17]Observational Cosmology Laboratory, Code 665, NASA Goddard Space Flight Center, Greenbelt, Maryland 20771, USA. [18]School of Physics and Astronomy, University of Nottingham, Nottingham NG7 2RD, UK. [19]School of Physics and Astronomy, Cardiff University, Queens Buildings, The Parade, Cardiff CF24 3AA, UK. [20]Dipartimento di Astronomia, Università di Padova, vicolo Osservatorio, 3, 35122 Padova, Italy. [21]Department of Astrophysical and Planetary Sciences, CASA 389-UCB, University of Colorado, Boulder, Colorado 80309, USA. [22]Department of Physics and Astronomy, University of British Columbia, 6224 Agricultural Road, Vancouver, British Columbia V6T 1Z1, Canada. [23]ESO, Karl-Schwarzschild-Strasse 2, 85748 Garching bei München, Germany. [24]UK Astronomy Technology Centre, Royal Observatory, Blackford Hill, Edinburgh EH9 3HJ, UK. [25]European Space Research and Technology Centre (ESTEC), Keplerlaan 1, 2201 AZ, Noordwijk, The Netherlands. [26]Institut d'Astrophysique Spatiale (IAS), bâtiment 121, Université Paris-Sud 11 and CNRS (UMR 8617), 91405 Orsay, France. [27]Infrared Processing and Analysis Center, MS 100-22, California Institute of Technology, JPL, Pasadena, California 91125, USA. [28]School of Physics and Astronomy, The University of Manchester, Alan Turing Building, Oxford Road, Manchester M13 9PL, UK. [29]Institut d'Astrophysique de Paris, UMR 7095, CNRS, UPMC Université Paris 06, 98 bis boulevard Arago, F-75014 Paris, France. [30]RAL Space, Rutherford Appleton Laboratory, Chilton, Didcot, Oxfordshire OX11 0QX, UK. [31]Institute for Space Imaging Science, University of Lethbridge, Lethbridge, Alberta T1K 3M4, Canada. [32]Department of Astrophysics, Denys Wilkinson Building, University of Oxford, Keble Road, Oxford OX1 3RH, UK. [33]CSIRO Astronomy and Space Science, PO Box 76, Epping, New South Wales 1710, Australia. [34]Centre for Astrophysics Research, University of Hertfordshire, College Lane, Hatfield, Hertfordshire AL10 9AB, UK. [35]Harvard-Smithsonian Center for Astrophysics, 60 Garden Street, Cambridge, Massachusetts 02138, USA.

Table 1 | 250 μm detection statistics in various regions of parameter space

Region of (z,L_X) parameter space	Number of AGN	Number of AGN associated with 250 μm sources	Expected number of spurious associations	Fraction of AGN associated with 250 μm sources
All z, 10^{42} erg s^{-1} $< L_X <$ 10^{45} erg s^{-1}	176	24	2.1	$14 \pm 3(^{+6}_{-5})$%
$1 < z < 3$, 10^{43} erg s^{-1} $< L_X <$ 10^{44} erg s^{-1}	44	11	0.5	$25^{+8}_{-7}(^{+15}_{-12})$%
$1 < z < 3$, 10^{44} erg s^{-1} $< L_X <$ 10^{45} erg s^{-1}	21	0	0.2	<5(<13)%

The first row corresponds to the entire sample of secure AGN in the CDF-N, while the second and third rows correspond to the regions enclosed within the blue dashed lines in Fig. 1. Confidence intervals on the fraction of AGN associated with 250 μm sources are given at 68%, with 95% intervals enclosed in brackets. It should be noted that there is one case of two AGN being associated with the same 250 μm source. The two AGN have very similar spectroscopic redshifts, and both have X-ray luminosities between 10^{43} and 10^{44} erg s^{-1}. Although the two AGN cannot be resolved at 250 μm, source extraction using X-ray and 24 μm positions as priors[25] indicates that both AGN are 5σ sources at 250 μm.

250 μm sources in annular regions of radius 10–30 arcsec around the X-ray source positions, and is reported in Table 1.

The distribution of CDF-N AGN in the redshift–X-ray luminosity (z–L_X) plane is shown in Fig. 1, and reveals a striking trend of 250 μm detectability with X-ray luminosity: of the 24 AGN detected at 250 μm, none of them have $L_X > 10^{44}$ erg s^{-1}. The redshift range between 1 and 3 is of most interest, because it corresponds to the epoch in which powerful AGN accreted most of their black hole mass and present-day massive galaxies formed most of their stars. Within this redshift range, Fig. 1 shows that 11 out of 44 AGN (25^{+8}_{-7}%) with 10^{43} erg s^{-1} $< L_X <$ 10^{44} erg s^{-1} are detected at 250 μm, while none of the 21 objects with $L_X > 10^{44}$ erg s^{-1} are detected. The difference in detection rates has a significance of >99%, according to a single-tail Fisher's exact test. We have considered the effects that incompleteness in the spectroscopic redshifts, or absorption of the X-ray flux by gas and dust, might have on our results. We find that the systematic non-detection of the powerful AGN is robust against both effects, although X-ray absorption does appear to be a common property of the AGN detected at 250 μm. We have also verified the low 250 μm detection rate of AGN with $L_X > 10^{44}$ erg s^{-1} using the Extended Chandra Deep Field South field, finding that of 49 such sources with $1 < z < 3$, only 1 is detected at 250 μm.

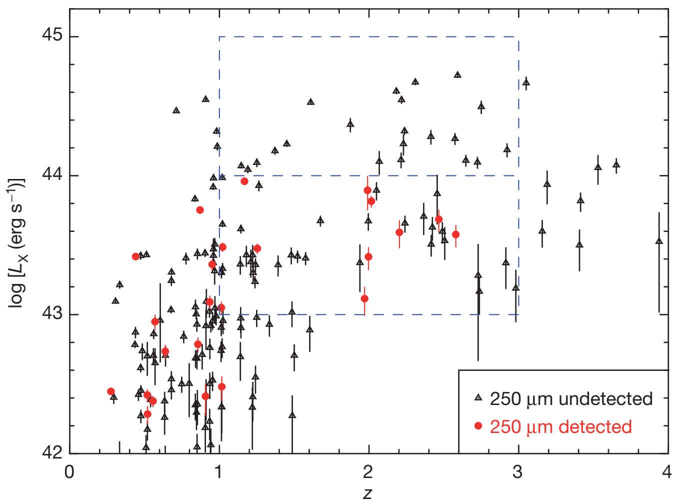

Figure 1 | Redshifts (z) and 2–8 keV X-ray luminosities (L_X) of AGN in the CDF-N. The luminosities have been corrected to the rest frame assuming a spectrum $S_\nu \propto \nu^{-0.9}$ and are not corrected for intrinsic absorption. The blue dashed rectangles delimit the luminosity decades above and below 10^{44} erg s^{-1} in the $1 < z < 3$ redshift range. Error bars, 68% confidence limits.

Infrared spectral energy distributions for the 250-μm-detected AGN were constructed by combining the SPIRE photometry with 3.6–160 μm photometry from the Spitzer Space Telescope. X-ray and infrared properties of the 11 250-μm-detected AGN with $1 < z < 3$ and L_X in the range 10^{43}–10^{44} erg s^{-1} are given in Table 2. In most cases, the AGN contributes less than 10% to the infrared luminosity. The best-fit infrared luminosities lie between 4×10^{11} and 10^{13} times solar luminosity ($L_\odot$), implying star formation rates between 50 and 1,750 solar masses ($M_\odot$) per year[18].

We performed a stacking analysis for the $1 < z < 3$ AGN to probe below the confusion limit of the SPIRE images. We split the sample into five bins of L_X from 10^{43} to 10^{45} erg s^{-1} and determined the average star formation rates of AGN in each bin. The results are shown in Fig. 2. In the redshift range $1 < z < 3$, the mean star formation rate in AGN with L_X of 10^{43}–10^{44} erg s^{-1} is 214 ± 25 $M_\odot$ per year, compared to a mean star formation rate for AGN with $L_X > 10^{44}$ erg s^{-1} of 65 ± 18 $M_\odot$ per year. These averages are independent of the SPIRE 250 μm detection limit because they are obtained from a stack of all sources within a given range of L_X, whether detected at 250 μm or not.

At redshifts of 1–3, the X-ray luminosity of 10^{44} erg s^{-1}, which divides the regions of 250 μm detection and non-detection in Fig. 1, corresponds approximately to the knee in the luminosity function of AGN[19]. The steep shape of the luminosity function at $L_X > 10^{44}$ erg s^{-1} implies that this part of the luminosity function is dominated by objects which are at the peak of their accretion rates. Our observations

Table 2 | Properties of SPIRE-detected AGN

ID	Redshift	Log[L_X (erg s^{-1})]	Log[N_H (atoms cm^{-2})]	Absorption correction	Log[L_{IR} ($L_\odot$)]	AGN (%)	SFR ($M_\odot$ yr^{-1})
35	2.203	$43.59^{+0.08}_{-0.11}$	$23.6^{+0.1}_{-0.2}$	$0.15^{+0.05}_{-0.07}$	12.70 ± 0.03	12	750–850
109	2.580	$43.58^{+0.07}_{-0.09}$	$23.4^{+0.1}_{-\text{unc}}$	$0.09^{+0.03}_{-0.09}$	13.01 ± 0.05	5	1,660–1,750
135	2.466	$43.69^{+0.07}_{-0.09}$	>24.0	>0.30	12.81 ± 0.05	4	1,060–1,110
158	1.013	$43.05^{+0.04}_{-0.05}$	$23.01^{+0.1}_{-0.1}$	$0.15^{+0.02}_{-0.02}$	12.29 ± 0.09	4	320–330
190	2.015	$43.81^{+0.04}_{-0.04}$	$23.6^{+0.1}_{-0.1}$	$0.16^{+0.02}_{-0.02}$	12.88 ± 0.03	21	1,030–1,300
331	1.253	$43.48^{+0.03}_{-0.04}$			12.51 ± 0.07	5	530–550
366	1.970	$43.11^{+0.08}_{-0.12}$	$23.4^{+0.1}_{-0.2}$	$0.11^{+0.03}_{-0.04}$	12.84 ± 0.05	3	1,140–1,170
368	1.996	$43.42^{+0.07}_{-0.09}$	>23.8	>0.26	12.41 ± 0.06	3	420–430
384	1.021	$43.49^{+0.03}_{-0.03}$	$23.4^{+0.1}_{-0.1}$	$0.25^{+0.02}_{-0.03}$	11.55 ± 0.17	11	50–60
455	1.168	$43.96^{+0.02}_{-0.02}$			11.97 ± 0.04	30	110–160
500	1.990	$43.89^{+0.10}_{-0.14}$	$23.2^{+0.2}_{-\text{unc}}$	$0.07^{+0.03}_{-0.07}$	12.62 ± 0.03	4	690–710

Data are given for AGN with $1 < z < 3$ and 10^{43} erg s^{-1} $< L_X <$ 10^{44} erg s^{-1}. The first column gives the ID number of the source in the X-ray catalogue[11]. The second column gives the redshift, and the third column gives the logarithm of the 2–8 keV X-ray luminosity (L_X). The fourth column gives the logarithm of the column density of absorbing gas (N_H, in units of hydrogen atoms per cm^2) implied by the ratio of 2–8 keV to 0.5–2 keV X-rays; a blank entry indicates no evidence for photoelectric absorption in X-rays, and 'unc' is used where the lower limit to the column density is unconstrained. The fifth column gives the correction to log L_X to account for the absorption. The sixth column gives the 8–1,000 μm infrared luminosity, L_{IR}. The seventh column gives the maximum likely contribution of an AGN to the infrared luminosity, and the eighth column gives the range of star formation rate (SFR) implied by the infrared luminosity, where the upper and lower limits correspond to zero AGN contribution and the maximum AGN contribution to the infrared luminosity, respectively. Photometry for the spectral energy distributions was extracted from Spitzer and SPIRE images using the X-ray and 24 μm catalogue positions as priors[25]. Total 8–1,000 μm infrared luminosities were then determined by fitting templates[26] to the spectral energy distributions[27]. Upper limits to the AGN contribution to the infrared luminosities were obtained by normalizing an AGN template in the mid-infrared[28].

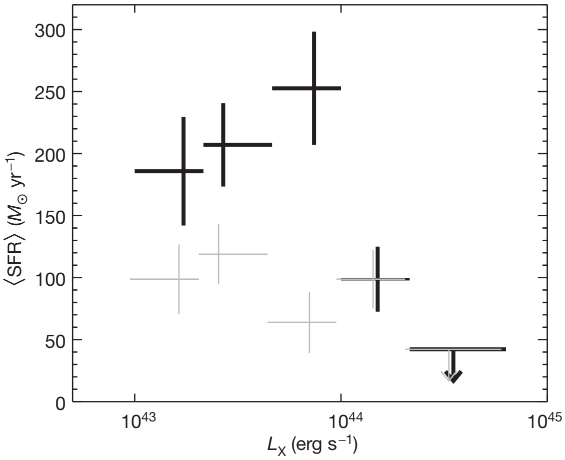

Figure 2 | Average star formation rates, ⟨SFR⟩, derived from averaged far-infrared luminosities of $1 < z < 3$ AGN, as a function of L_X. We converted the 250, 350 and 500 μm flux densities for each source into an equivalent 8–1,000 μm luminosity by fitting a grey-body curve, with a temperature of 30 K in the rest-frame of the source, an emissivity index of $\beta = 1.6$, and a power-law extension to the Wien side[29] and multiplying by $4\pi D_L^2$, where D_L is the luminosity distance. Fluctuations in the map sometimes scatter the fluxes of undetected sources to negative values, which translate to negative luminosities when multiplied by $4\pi D_L^2$. Such negative solutions for individual AGN were allowed so as not to produce an artificial positive bias in the averages. The luminosities were averaged in five bins in L_X, which were chosen to include a similar number of AGN in each bin. The average luminosities were then converted to star formation rates[18]. AGN which are individually detected at 250 μm are included in the averages shown in bold black, but have been excluded from the averages which are shown in grey, to show the contribution that these sources make to the average star formation rates. The grey points have been offset horizontally from the bold black points for clarity. Error bars correspond to 68% confidence limits and were determined by bootstrap resampling, with a 7% systematic error added in quadrature to account for the calibration error on SPIRE photometry.

therefore imply that the most prodigious episodes of star formation are common in the host galaxies of $1 < z < 3$ AGN, but avoid powerful AGN in which accretion is at its peak.

This systematic non-coincidence of the peak periods of star formation and accretion implies a direct interaction between the two processes, and provides a powerful discriminator for the form of AGN feedback which is responsible for terminating star formation in the host galaxy. Two families of feedback models have been proposed, widely referred to as 'quasar mode' and 'radio mode'[20]. In quasar-mode feedback, a luminous AGN generates a powerful wind which terminates star formation by driving the interstellar medium from the surrounding host galaxy. In radio-mode feedback, star formation is suppressed because collimated jets of relativistic particles emitted by a radiatively inefficient AGN prevent gas in the surrounding hot halo from cooling, thereby starving the galaxy of cool gas from which to form stars.

Radio-mode feedback is commonly invoked in semi-analytical models to limit galaxy masses and luminosities[20,21]. In these models, black holes grow through luminous accretion episodes and black hole mergers. The correlation between black hole mass and bulge mass comes from assuming that a fixed fraction of the gas is accreted by the nucleus during each star forming episode that results from a galaxy merger or disc instability, and hence star formation and accretion rate should be correlated over the full range of luminosity. Our observations are therefore inconsistent with models in which AGN influence their host galaxies only through radio-mode feedback[20,21]. In contrast, models of galaxy formation in which quasar-mode feedback is responsible for terminating the star formation[7,8,9,22], and which have received some observational support recently[23,24], predict that the AGN luminosity peaks later than the star formation rate, and thus are consistent with our observations. These models also predict that residual star formation, at the level of a few tens of per cent of the peak, will continue during the period in which the AGN luminosity is at its maximum, consistent with our stacked results; our results show that, on average, AGN with $L_X > 10^{44}$ erg s^{-1} are still forming stars at approximately 65 $M_\odot$ per year. Our observations do not discriminate between models invoking major mergers[8] or accretion of gas into a massive halo[22] as the trigger for the intense star formation. After the interstellar medium has been driven out by the luminous AGN and the AGN itself becomes starved of fuel, radio-mode feedback is the most credible agent by which further star formation is inhibited.

Received 30 November 2011; accepted 29 March 2012.

1. Häring, N. & Rix, H. W. On the black hole mass-bulge mass relation. *Astrophys. J.* **604,** L89–L92 (2004).
2. Silk, J. & Rees, M. J. Quasars and galaxy formation. *Astron. Astrophys.* **331,** L1–L4 (1998).
3. Fabian, A. C. The obscured growth of massive black holes. *Mon. Not. R. Astron. Soc.* **308,** L39–L43 (1999).
4. King, A. R. Black hole outflows. *Mon. Not. R. Astron. Soc.* **402,** 1516–1522 (2010).
5. Brandt, W. N. & Hasinger, G. Deep extragalactic X-ray surveys. *Annu. Rev. Astron. Astrophys.* **43,** 827–859 (2005).
6. Sanders, D. B. & Mirabel, I. F. Luminous infrared galaxies. *Annu. Rev. Astron. Astrophys.* **34,** 749–792 (1996).
7. Di Matteo, T., Springel, V. & Hernquist, L. Energy input from quasars regulates the growth and activity of black holes and their host galaxies. *Nature* **433,** 604–607 (2005).
8. Springel, V., Di Matteo, T. & Hernquist, L. Modelling feedback from stars and black holes in galaxy mergers. *Mon. Not. R. Astron. Soc.* **361,** 776–794 (2005).
9. Sijacki, D., Springel, V., Di Matteo, T. & Herhquist, L. A unified model for AGN feedback in cosmological simulations of structure formation. *Mon. Not. R. Astron. Soc.* **380,** 877–900 (2007).
10. Hatziminaoglou, E. *et al.* HerMES: far infrared properties of known AGN in the HerMES fields. *Astron. Astrophys.* **518,** L33 (2010).
11. Alexander, D. M. *et al.* The Chandra Deep Field North Survey. XIII. 2 Ms point-source catalogs. *Astron. J.* **126,** 539–574 (2003).
12. Trouille, L., Barger, A. J., Cowie, L. L., Yang, Y. & Mushotzky, R. F. The OPTX Project. I. The flux and redshift catalogs for the CLANS, CLASXS, and CDF-N fields. *Astrophys. J.* **179** (Suppl.), 1–18 (2008).
13. Barger, A. J. *et al.* A highly complete spectroscopic survey of the GOODS-N field. *Astrophys. J.* **689,** 687–708 (2008).
14. Mateos, S. *et al.* XMM-Newton observations of the Lockman Hole IV: spectra of the brightest AGN. *Astron. Astrophys.* **444,** 79–99 (2005).
15. Griffin, M. J. *et al.* The Herschel-SPIRE instrument and its in-flight performance. *Astron. Astrophys.* **518,** L3 (2010).
16. Oliver, S. J. *et al.* HerMES: SPIRE galaxy number counts at 250, 350, and 500 μm. *Astron. Astrophys.* **518,** L21 (2010).
17. Smith, A. J. *et al.* HerMES: point source catalogues from deep Herschel-SPIRE observations. *Mon. Not. R. Astron. Soc.* **419,** 377–389 (2012).
18. Kennicutt, R. C. The global Schmidt law in star-forming galaxies. *Astrophys. J.* **498,** 541–552 (1998).
19. Ebrero, J. *et al.* The XMM-Newton serendipitous survey. VI. The X-ray luminosity function. *Astron. Astrophys.* **493,** 55–69 (2009).
20. Croton, D. J. *et al.* The many lives of active galactic nuclei: cooling flows, black holes and the luminosities and colours of galaxies. *Mon. Not. R. Astron. Soc.* **365,** 11–28 (2006).
21. Bower, R. G. *et al.* Breaking the hierarchy of galaxy formation. *Mon. Not. R. Astron. Soc.* **370,** 645–655 (2006).
22. Granato, G. L. *et al.* A physical model for the coevolution of QSOs and their spheroidal hosts. *Astrophys. J.* **600,** 580–594 (2004).
23. Farrah, D. *et al.* Direct evidence for termination of obscured star formation by radiatively driven outflows in reddened QSOs. *Astrophys. J.* **745,** 178 (2012).
24. Cano-Díaz, M. *et al.* Observational evidence of quasar feedback quenching star formation at high redshift. *Astron. Astrophys.* **537,** L8 (2012).
25. Roseboom, I. G. *et al.* The Herschel Multi-Tiered Extragalactic Survey: source extraction and cross-identifications in confusion-dominated SPIRE images. *Mon. Not. R. Astron. Soc.* **409,** 48–65 (2010).
26. Siebenmorgen, R. & Krügel, E. Dust in starburst nuclei and ULIRGs. SED models for observers. *Astron. Astrophys.* **461,** 445–453 (2007).
27. Symeonidis, M. *et al.* The link between SCUBA and Spitzer: cold galaxies at z ≤ 1. *Mon. Not. R. Astron. Soc.* **397,** 1728–1738 (2009).
28. Seymour, N. *et al.* HerMES: SPIRE emission from radio-selected active galactic nuclei. *Mon. Not. R. Astron. Soc.* **413,** 1777–1786 (2011).
29. Blain, A. W., Barnard, V. E. & Chapman, S. C. Submillimetre and far-infrared spectral energy distributions of galaxies: the luminosity-temperature relation and consequences for photometric redshifts. *Mon. Not. R. Astron. Soc.* **338,** 733–744 (2003).

Supplementary Information is linked to the online version of the paper at www.nature.com/nature.

Acknowledgements Herschel is an ESA space observatory with science instruments provided by European-led Principal Investigator consortia and with important participation from NASA. SPIRE has been developed by a consortium of institutes led by Cardiff University (UK) and which includes: University of Lethbridge (Canada); NAOC (China); CEA, LAM (France); IFSI, University of Padua (Italy); IAC (Spain); Stockholm Observatory (Sweden); Imperial College London, RAL, UCL-MSSL, UKATC, University of Sussex (UK); and Caltech, JPL, NHSC, University of Colorado (USA). This development has been supported by national funding agencies: CSA (Canada); NAOC (China); CEA, CNES, CNRS (France); ASI (Italy); MCINN (Spain); SNSB (Sweden); STFC, UKSA (UK); and NASA (USA).

Author Contributions This Letter represents the combined work of the HerMES collaboration, the SPIRE Instrument Team's extragalactic survey. M.J.P. planned the study, and wrote the draft version of the paper. M.S. fitted models to the spectral energy distributions of the sources and J.D.V. performed the stacking analysis. All other co-authors contributed extensively and equally by their varied contributions to the SPIRE instrument, the Herschel mission, analysis of SPIRE and HerMES data, planning of HerMES observations and scientific support of HerMES, and by commenting on this manuscript as part of an internal review process.

Author Information Reprints and permissions information is available at www.nature.com/reprints. The authors declare no competing financial interests. Readers are welcome to comment on the online version of this article at www.nature.com/nature. Correspondence and requests for materials should be addressed to M.J.P. (mjp@mssl.ucl.ac.uk).